ACS APPLIED MATERIALS & INTERFACES

Research Article

www.acsami.org

Electrodeposition of Nanoflake Pd Structures: Structure-Dependent Wettability and SERS Activity

Hwakyeung Jeong and Jongwon Kim*

Department of Chemistry, Chungbuk National University, Cheongju, Chungbuk 361-763, Korea

Supporting Information

ABSTRACT: The characteristic properties of metal surfaces, i.e., wettability and surface-enhanced Raman scattering (SERS) activity, have been the subject of intensive research because of their useful applications. In the present work, we report a simple electrodeposition of nanoflake Pd structures onto clean Au surfaces without the use of additives. The fine structure of the nanoflake Pd surfaces was regulated by controlling the deposition charge, and the effect of the structural variations on the wettability and SERS activity was examined. The wettability of nanoflake Pd structures in terms of water contact angle was closely related to the fine structures of Pd deposits and their surface roughness. The SERS activity of the nanoflake Pd surfaces was highly dependent on the presence of sharp edge sites on the Pd structures. Well-defined nanoflake Pd structures prepared using a deposition charge of 0.04 C exhibited superhydrophobic natures and reproducible SERS activity. The effect of the metal surface structures on the wettability and the SERS activity demonstrated in this work provides insight into the fabrication of functional metal nanostructures.

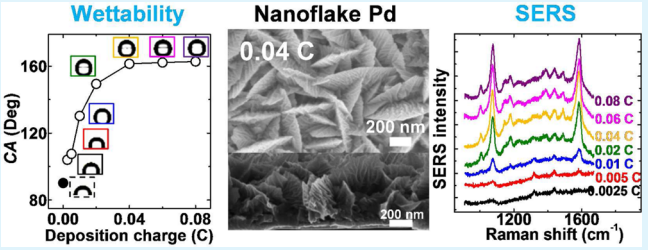

KEYWORDS: *electrodeposition, nanoflake Pd, wettability, surface roughness, surface-enhanced Raman scattering*

1. INTRODUCTION

Because nanostructured metal surfaces exhibit unique physical and chemical properties that differ from those of the bulk-state metals, these surfaces provide useful applications in heterogeneous catalysis, biosensors,[1] electronics,[2] and electrocatalysis.[3−5] The specific properties of nanostructured metal surfaces can be controlled by their shapes and sizes; therefore, the fabrication of well-defined nanostructured metal surfaces has been the subject of intensive research.[2] Solution-based syntheses of metal nanoparticles and their assemblies have been successfully used in diverse applications; however, the fabrication procedures involve multiple steps and are time-consuming.[6,7] Recently, electrochemical deposition methods have received significant attention as a straightforward route for the fabrication of nanostructured metal surfaces.[8,9] In addition to the simplicity of the fabrication protocols, the electrodeposition methods provide clean nanostructured metal surfaces that are free of capping-agent or linker molecules that are inevitable in the assembly of solution-dispersed metal nanoparticles.[8]

Among the various applications of nanostructured metal surfaces, the control of the wetting properties of nanostructured metal surfaces to achieve superhydrophobicity or superhydrophilicity has received significant attention because the wettability of solid surfaces is important in many technological fields, such as the fabrication of self-cleaning materials, the manipulation of biomaterials, and microfluidics.[10,11] Because most metals and metal oxides have high surfaces energies, flat metal surfaces exhibit low water contact angles, whereas roughened metal surfaces modified with a low-surface-energy self-assembled monolayer exhibit higher contact angles.[12,13] The electrodeposition of metal nanostructures has been demonstrated to be effective for fabricating hydrophobic surface structures.[14,15] Flower-like Au microstructures electrodeposited onto indium tin oxide substrates exhibited superhydrophobic natures.[14,16] Nanostructured Pt and Cu surfaces prepared by electrodeposition methods have been shown to exhibit superhydrophobicity.[13,17]

Another important application of nanostructured metal surfaces is their use as surface-enhanced Raman scattering (SERS) substrates. Because of the large signal amplification at nanostructured metal surfaces, SERS is useful in various applications, including biological sensing and trace analysis.[18,19] The electrodeposition of metal nanostructured surfaces is an effective method for preparing reproducible SERS-active substrates. In the case of SERS-active coinage-metal species, such as Au and Ag, electrodeposited nanostructures have been successfully used to fabricate highly SERS-active substrates.[20−22] It was also reported that Pt and Pd nanostructured surfaces prepared by electrodeposition methods can be served as SERS-active substrates, although these metals are less SERS active.[23−25]

Both of these characteristic properties of metal surfaces, i.e., wettability and SERS activity, are dependent on the detailed

Received: December 16, 2014
Accepted: March 19, 2015
Published: March 19, 2015

DOI: 10.1021/acsami.5b02113
ACS Appl. Mater. Interfaces 2015, 7, 7129−7135

shape and size of metal nanostructures. Several recent investigations focused on the fabrication of metal nanostructures for controlling the wettability and SERS activity of metal surfaces. Zhou and co-workers investigated the surface wettability and SERS activity of hierarchical Pt nanostructures and observed that flower-like Pt structures exhibited higher activities compared to those of spherical structures.[15] Ling and co-workers reported the fabrication of superhydrophobic SERS platforms for trace molecular sensing via assembly of Ag nanocubes.[26] Nakanishi and co-workers prepared nanoflake-Au surfaces and examined their wettability and SERS activities.[27] Despite the previous works regarding either wettability or SERS activity of nanostructured metal surfaces, most of these works have been focused on the fabrication of specific surface nanoarchitectures and evaluation of their surface functionalities. Moreover, the dependence of wettability and SERS activity on the variation of fine structure of metal surfaces has not been previously examined in a systematic way. In this work, we report on the fabrication of flake-type Pd nanostructures using simple electrodeposition onto clean Au surfaces without additives or premodification of the substrate surfaces. The fine shape of the Pd electrodeposits were regulated by controlling the total charge during the electrodeposition, and the effect of the surface structures on the wettability and SERS activity was systematically examined.

2. EXPERIMENTAL SECTION

All solutions were prepared using purified water (Milli-Q, 18.2 MΩ·cm). K_2PdCl_4 was purchased from Alfa Aesar, and all other chemicals were purchased from Aldrich. A CHI 660C (CH Instruments) was used in all electrochemical measurements. Pt-wire and Ag/AgCl electrodes were used as counter and reference electrodes, respectively. All potentials are reported relative to the Ag/AgCl reference electrode (3 M NaCl). Au films evaporated onto silicon (Au/Si) wafers (KMAC, Korea) were used as substrates for electrodeposition. After the Au/Si substrate was cleaned for 1 min in a piranha solution, it was confined in a Viton O-ring with an inner diameter of 2.9 mm and used as the working electrode. ***Caution***: piranha solution is aggressive and explosive. Never mix piranha waste with solvents. Check the safety precautions before using it. The electrodeposition was performed in a constant-potential mode from solutions containing K_2PdCl_4 (typically 5 mM for well-defined structures) and 0.1 M H_2SO_4. Scanning electron microscopy (SEM) characterization was performed using an ULTRA PLUS field-emission scanning electron microscope (Carl Zeiss). Contact-angle measurements using 5 μL sessile water drops were performed using a Phoenix 300 system (Surface & Electro-Optics Co., Korea). The SERS spectra were obtained using a homemade Ramboss micro-Raman system spectrometer equipped with an integral microscope (Olympus BX 51 with a 20X long distance objective lens). Radiation of 632.8 nm from an air-cooled He/Ne laser with a radiation power of 8.5 mW was used as an excitation source.

3. RESULTS AND DISCUSSION

3.1. Effect of the Deposition Conditions on the Morphology of the Pd Nanostructures. The effect of the deposition conditions on the morphology of the Pd nanostructures was first examined. Figure 1 shows SEM images of Pd nanostructures electrodeposited at various deposition potentials from solutions containing 5 mM K_2PdCl_4 + 0.1 M H_2SO_4 with a deposition charge of 0.02 C. When negative deposition potentials (−0.3 to −0.15 V) were applied, spike-type Pd nanostructures grew vertically. As the deposition potentials were adjusted in the positive direction, the dimensions of the Pd nanostructures decreased and became more uniform. Flake-type Pd nanostructures were formed with

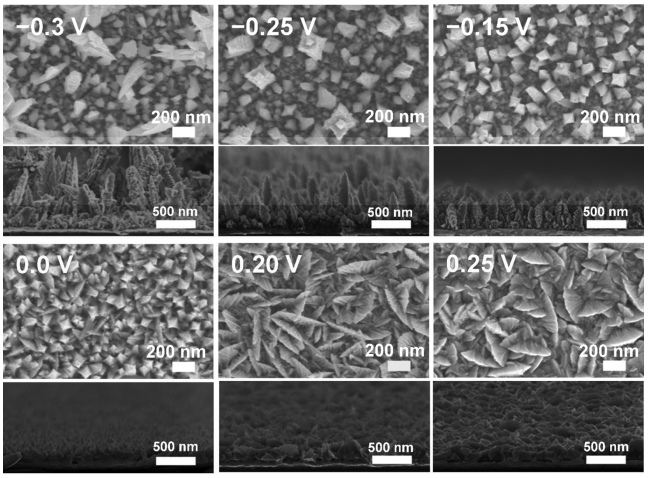

Figure 1. Top and cross-sectional SEM images of Pd nanostructures electrodeposited from solutions containing 5 mM K_2PdCl_4 + 0.1 M H_2SO_4 at various deposition potentials. The total deposition charge was 0.02 C.

applied potentials between 0.20 and 0.25 V, which are significantly different from the spike-type Pd structures. The surfaces of the Pd flakes retained wrinkled structures, resembling cabbage leaves.

In our previous work, it was reported that triangular Pd rod structures were obtained by electrodeposition at −0.1 V from a solution containing 15 mM K_2PdCl_4 and 0.1 M H_2SO_4. The spike-type Pd nanostructures obtained at negative potential regions are considered to have growth patterns similar to those of the triangular Pd rods because they grew anisotropically in the vertical direction. In contrast, the Pd structures observed at approximately 0.2 V are flake-type and differ from the previously reported rod-type structures. The adsorption of H at the electrodeposited Pd surfaces at potentials more negative than 0 V may play a role determining different structures of Pd deposits.

The applied potential of 0.20 V required for the formation of Pd flake structures is slightly more negative than the standard reduction potential of $PdCl_4^{2-}$ (aq)/Pd(s) (0.40 V vs Ag/AgCl).[28] The electrodeposition of Au at potentials slightly more negative than its standard reduction potential has been reported to result in flake-type Au nanostructures.[14,29] In both cases, deposition potentials close to the standard reduction potentials maintain a relatively slow reduction rate, which results in the formation of flake-type nanostructures. Another experimental variable affecting the reduction rate is the concentration of the precursors; thus, the effect of the deposition potentials and precursor concentrations on the morphology of the resulting Pd nanostructures was systematically examined (Figure S1 of the Supporting Information). Flake-type Pd nanostructures were obtained when relatively positive potentials were applied, where lower precursor concentrations favored the formation of well-defined flake-type Pd nanostructures.

The electrodeposition of flake-type Pd nanostructures has been previously reported; however, the addition of surfactants such as cetyltrimethylammonium bromide[30] or premodification of the substrate with polymer layers[31] was required for the formation of Pd flake structures. In the present work, well-defined nanoflake Pd structures were electrodeposited onto a clean Au surface without any additives, which was possible at

DOI: 10.1021/acsami.5b02113
ACS Appl. Mater. Interfaces 2015, 7, 7129−7135

slow reduction rates under positive applied deposition potentials when low precursor concentrations were used. As described in the follow sections, we examined the structural variation of the flake-type Pd nanostructures as a function of the deposition charges as well as the effect of the surface structures on the wettability and SERS activity.

3.2. Effect of the Deposition Charges on the Morphologies of the Pd Nanostructures. The growth of nanoflake Pd structures was monitored by varying the total deposition charge during electrodeposition at 0.20 V in 5 mM K_2PdCl_4 + 0.1 M H_2SO_4 (Figure 2). At an early deposition stage, the deposition current quickly decreased, which corresponds to the double-layer charging process and the initial electrodeposition of Pd layers. Even at the very early stage of electrodeposition (0.0025 C), the Au substrate surfaces were completely covered by Pd layers, as indicated by the absence of Au oxide layers in the cyclic voltammograms (Figure S2 of the Supporting Information). The subsequent current gradually increased to 0.04 C and then remained constant at ~22 μA. Flake-shaped Pd protrusions started to form with deposition charges of ca. 0.005 C, and the nanoflakes then grew anisotropically to form well-defined nanoflake Pd structures at 0.04 C. The thicknesses of the nanoflake Pd structures were typically ca. 20 nm, and their widths varied from 500 to 800 nm. The surfaces of the nanoflake Pd exhibited wrinkled structures that resemble cabbage leaves. The application of additional deposition charge resulted in an increase in the thickness of the Pd flakes, whereas their dimensions did not increase further (see also cross-sectional images). The cross-sectional SEM images show that the heights of the nanoflake Pd structures increased as the deposition charge increased to 0.04 C, after which the heights remained at similar levels of ~1 μm. Energy-dispersive X-ray analysis verified the Pd element of nanoflake Pd structures (Figure S3 of the Supporting Information)

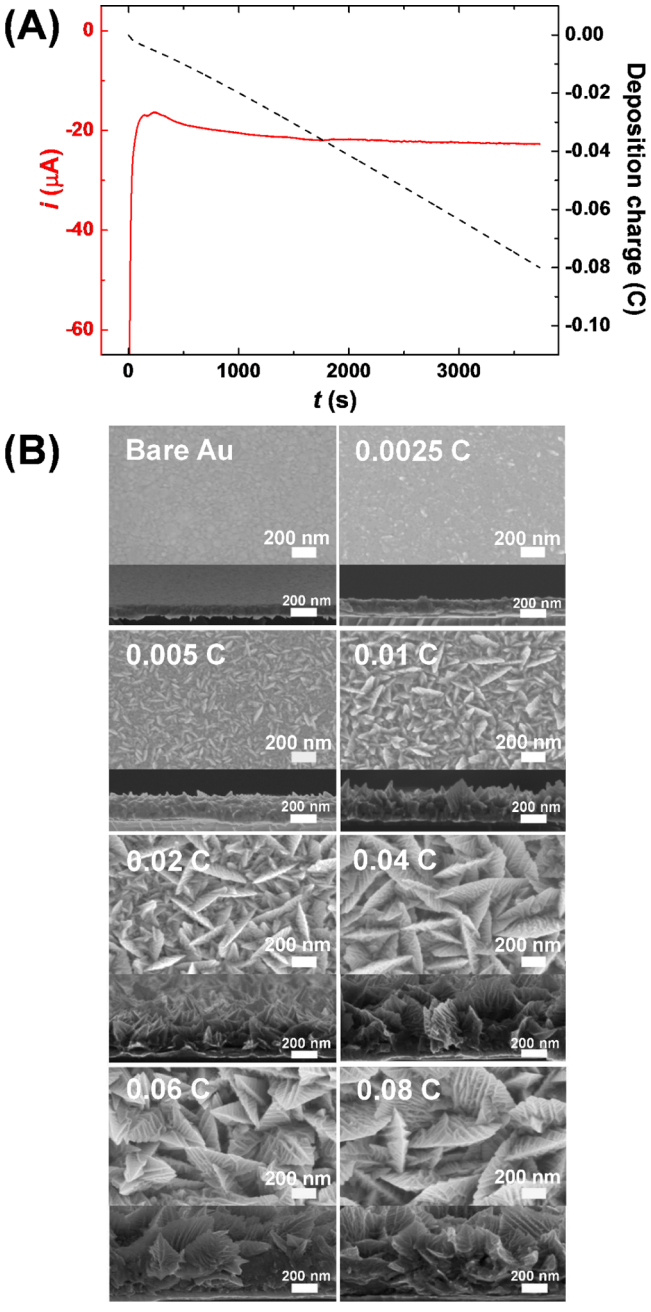

Figure 2. (A) Current and deposition charge vs time curve during electrodeposition at 0.20 V in 5 mM K_2PdCl_4 + 0.1 M H_2SO_4. (B) Top and cross-sectional SEM images as a function of deposition charge.

The surface area of the flake Pd nanostructures was measured using electrochemical methods. The cyclic voltammograms of the Pd flake nanostructures exhibit hydrogen adsorption/desorption and Pd oxide formation/reduction peaks in the negative and positive potential regions, respectively, which are characteristically observed in voltammograms of Pd surfaces (Figure 3A). The electrochemical surface area (ESA) of the nanostructured Pd surfaces was evaluated by integrating the charge consumed for the reduction of the surface oxide layer.[32] The roughness factor (R_f, ESA divided by the geometric area of the electrode surface) of the Pd nanostructures gradually increased as the deposition charge increased to 0.04 C (Figure 3B). The R_f-value of well-defined nanoflake Pd structures (0.04 C) was 9.8, and no further increase in R_f was observed with extended deposition charges. The previously discussed SEM images revealed that further application of deposition charge beyond 0.04 C resulted in an increase in the thicknesses of the Pd nanoflakes, which did not affect the R_f of the nanoflake Pd surfaces.

3.3. Water Contact Angle at Nanoflake Pd Surfaces. We first examined the wettabilities of the Pd nanostructures electrodeposited with different deposition charges. Figure 4 shows the dependence of the water contact angle (CA) at the Pd nanostructures as a function of the deposition charge. After Pd was electrodeposited (0.005 C) onto the Au surfaces, the CA increased to 104° from the CA of 90° obtained for flat Pd surfaces. The CA then quickly increased as the deposition charge was increased to 0.02 C, where superhydrophobic surfaces with CA of 150° were achieved. At 0.04 C of deposition charge, the CAs of the nanostructures were measured to be 161°, and no further increase in the CA was observed with increasing deposition charge. The change in the CA at Pd surfaces without surfaces modification using *n*-dodecanethiol was also monitored, where the CA remained at ~60° irrespective of the deposition charge (Figure S4 of the Supporting Information).

The trend of the wettability with deposition charge shown in Figure 4 is very similar to that of the R_f change of the nanoflake Pd surfaces (Figure 3B). It is well-known that the wettability of solid surfaces is significantly affected by the surface roughness.[33]

DOI: 10.1021/acsami.5b02113
ACS Appl. Mater. Interfaces 2015, 7, 7129−7135

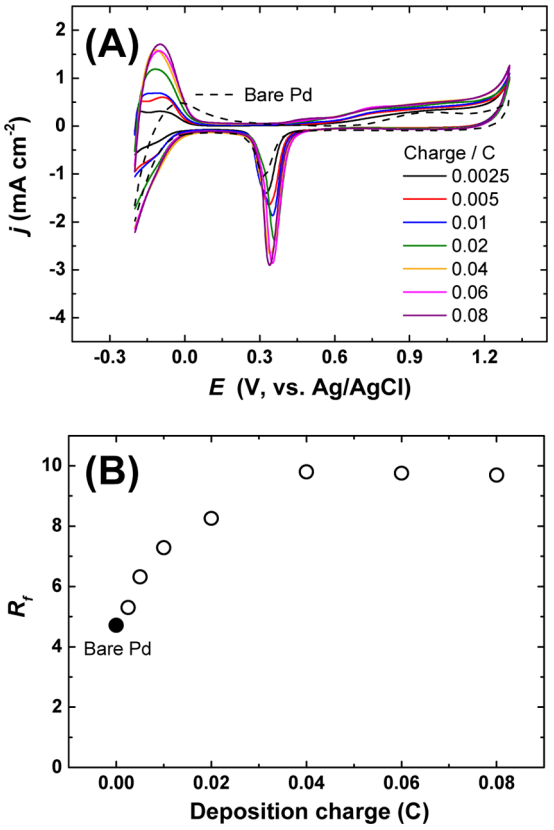

Figure 3. (A) Cyclic voltammograms obtained in 0.1 M $HClO_4$ on Pd nanostructures electrodeposited using different deposition charges. Scan rate: 50 mV/s. (B) Dependence of the R_f of Pd deposits on the deposition charge.

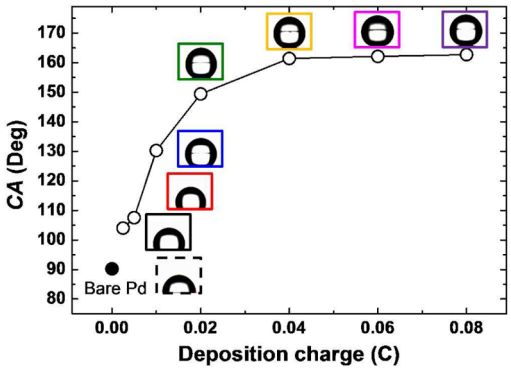

Figure 4. Contact-angle profiles of water droplets (5 μL) on nanostructured Pd surfaces modified with *n*-dodecanethiol as a function of deposition charge.

Two distinct hypotheses have been suggested to describe the correlation between the surface roughness and the wettability.[10,15−17,34] According to Wenzel's model, a water droplet can wet the entire microstructure surface; thus, no air is trapped between the water and the solid. In this case, the surface roughness (r, the ratio between the actual and apparent surface area) is related to the water CA measured on a rough surface (θ_r) and the intrinsic CA on a flat surface (θ):

$$\cos\theta_r = r\cos\theta \quad (1)$$

The surface roughness of the nanoflake Pd surfaces evaluated using eq 1 ranges from 50 to 220 depending on the deposition charge. These surface roughness r values are much greater than the R_f values (5−10) obtained from the ESA measurements, which implies that the entire surface of the Pd flake structure is not completely wetted by the water droplets.

In Cassie's model, the water droplet is suspended on the top of the asperities and the air fraction present between the surface and the water droplet make its suspension much easier. In this case, the water CA (θ_r and θ) can be related to the fractional interfacial areas of the water−solid (f_1) and the water−air (f_2) in the interspaces among the nanostructured surfaces (i.e., $f_1 + f_2 = 1$):

$$\cos\theta_r = f_1\cos\theta - f_2 \quad (2)$$

We evaluated the fractional interfacial areas of the water−air ($f_2 = 1 - f_1$) in the interspaces among the nanoflake Pd surfaces as a function of the deposition charge. Figure 5A shows

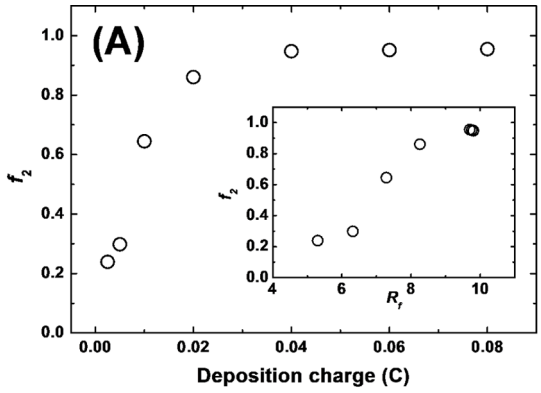

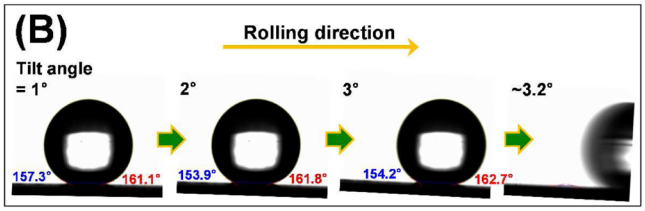

Figure 5. (A) Dependence of f_2 values of the nanostructured Pd surfaces on the deposition charge and roughness factor (R_f, inset). (B) Snapshot of the rolling off water droplet according to the tilting angles on nanoflake Pd surfaces (0.04 C) modified with *n*-dodecanethiol.

that the f_2 values steeply increase with as deposition charge is increased to 0.02 C, implying that the fractional interfacial areas of the water−air significantly increase. At deposition charges greater than 0.04 C, the f_2 values remained at the same level of 0.95. The correlation between f_2 and R_f is shown in the inset of Figure 5A, where the f_2 values increase with increasing roughness factor R_f.

As shown in the charge-dependent SEM images (Figure 2B), flake-type Pd structures continuously grew as the deposition charge was increased to 0.02 C. In this charge range, the surface roughness steeply increased, resulting in a quick increase in the CA values. After the deposition charge of 0.04 C, the R_f remained at the same levels; thus, no further increase in the CA was observed. The authors of previous investigations have reported the dependence of the CA at electrodeposited nanostructured metal surfaces as a function of the deposition charges.[35,36] In these previous works, the structures of the metal deposits and the surface coverage of the metal on the substrates significantly changed with the deposition charge. In the present

DOI: 10.1021/acsami.5b02113
ACS Appl. Mater. Interfaces 2015, 7, 7129−7135

work, we examined the effect of the variation in the fine structure of the Pd deposits on the CA, which is correlated to the R_f, of the nanoflake Pd structures.

To investigate further the hydrophobic nature of nanoflake Pd surfaces, we performed tilting experiments to measure CA hysteresis based on tilted plate methods.[37] Figure 5B shows the changes of left and right CAs depending on the tilt angle of the nanoflake Pd substrates. The water drop started to move at 3° of tilt angle, where the left and right CAs are assumed to be receding (θ_r) and advancing (θ_a) CAs, respectively. The CA hysteresis ($\theta_H = \theta_a - \theta_r$) at nanoflake Pd surfaces was measured to be 8.5°. The low CA hysteresis smaller than 10° and high static CA shown above indicate the superhydrophobic nature of nanoflake Pd surfaces.[38]

3.4. SERS Activity on the Nanoflake Pd Surfaces. We next investigated the utility of the nanoflake Pd structures as SERS-active substrates. To examine the effect of the structural change of the Pd nanostructures on the SERS activity, 4-aminobenzenethol (4-ABT) was adsorbed onto nanostructured Pd surfaces prepared with different deposition charges and their SERS spectra were obtained (Figure S5 of the Supporting Information). Comparing the SERS activities between substrates with different surface roughness, it should be noted that the SERS intensity depends on the amount of molecules adsorbed onto the surfaces, which is affected by the roughness of each substrate.[39] Therefore, we normalized the SERS intensity with respect to the R_f value of each Pd surface; the R_f-normalized SERS spectra are compared in Figure 6A. No SERS activity was observed on the flat Pd surfaces, whereas Pd nanostructures prepared with a deposition charge of 0.01 C exhibited considerable SERS activity. Nanoflake Pd structures prepared using greater deposition charges exhibited a significantly higher SERS activity, and a maximum was obtained for Pd nanoflakes with a deposition charge of 0.04 C.

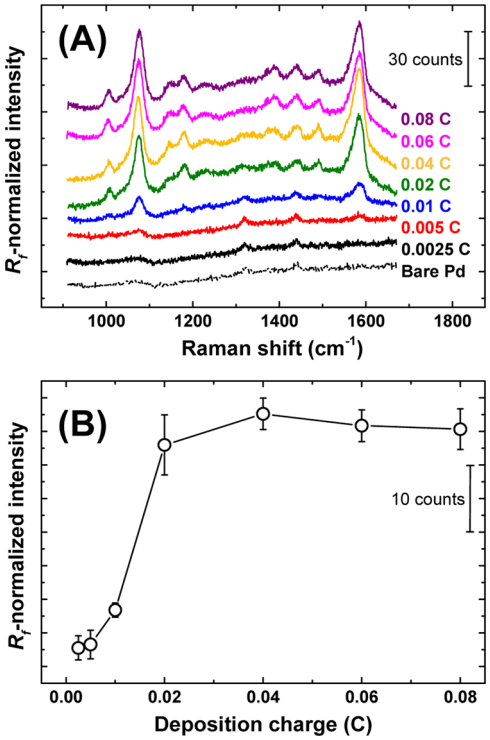

Figure 6. (A) R_f-normalized SERS spectra of 4-aminobenzenethiol adsorbed onto nanostructured Pd surfaces with different deposition charges. Acquisition time = 10 s. (B) Dependence of R_f-normalized SERS intensities at 1585 cm^{-1} on the deposition charge. The Pd substrates were soaked in 8 mM 4-aminobenzenethiol in ethanol for 12 h and rinsed with ethanol before the SERS measurements.

To show the trend of the SERS activity change at the Pd nanostructures, R_f-normalized SERS intensities at 1585 cm^{-1} are plotted as a function of the deposition charge in Figure 6B. The SERS activity steeply increased as the deposition charge increased from 0.005 to 0.02 C, and the activity then slightly increased to its maximum. When the deposition charge exceeded 0.04 C, the SERS activity slightly decreased. It is noteworthy that a sharp increase in SERS activity at Pd nanostructures was observed when the deposition charge increased from 0.01 to 0.02 C. It has been reported that the SERS activity at nanostructured metal surfaces is highly dependent on the presence of sharp edge sites, where large enhancements in the localized electromagnetic field are available for inducing SERS activity.[20,40−43] As shown in the SEM images of Figure 2B, Pd protrusions started to form at a deposition charge of 0.01 C and nanoflake Pd structures with sharp edge sites fully developed at 0.02 C. Additionally, winkle-like structures appeared on the sidewalls of nanoflake Pd structures. These structural changes in the Pd nanostructures resulted in a sudden increase in the SERS intensity of the nanoflake Pd structures at 0.02 C. Wrinkled nanoflake Pd structures were more defined at 0.04 C, with greater overall dimensions; however, only a slight increase in the SERS activity was observed.

To quantitatively estimate the SERS activity, the SERS enhancement factor (EF) was evaluated using the method developed by Tian et al.[20,44] The SERS EF for the nanoflake Pd structures deposited with a charge of 0.04 C was calculated to be 1.5×10^3, which is comparable to those of other highly SERS-active Pd nanostructures.[42,45−47] In addition to the high SERS activity, the reproducibility of the SERS intensities is an important characteristic for the application of SERS-active substrates.[48] The SERS reproducibility of well-defined nanoflake Pd structures (0.04 C) is demonstrated by uniform intensities in the SERS spectra collected at five random points from one nanoflake Pd substrate (Figure S6 of the Supporting Information). The reproducible SERS activity observed on electrodeposited Pd nanostructures was be verified by the small error bars included in Figure 6B. We also obtained SERS mapping images of nanoflake Pd surfaces (Figure S7 of the Supporting Information), wherein the deviations in SERS intensities were less than 5%. Homogeneous SERS intensities were measured at the whole electrodeposited area inside O-ring (diameter of 2.9 mm). This good SERS reproducibility is attributed to the uniform surface morphology of the electrodeposited nanoflake Pd structures (Figure S8 of the Supporting Information), which resulted in a homogeneous distribution of the active sites responsible for the SERS enhancement induced by the laser spot (~2 μm). The applicability of the nanoflake Pd substrates to electrochemical environments was also examined by obtaining potential-dependent SERS spectra of pyridine adsorbed onto the nanoflake Pd surfaces (Figure S9A of the Supporting Information). The SERS intensities of the ring-breathing mode (~1010 cm^{-1}) of pyridine exhibited a reversible and stable pattern under potential excursions (Figure S9B of the Supporting Information), which suggests that the nanoflake Pd substrates can be utilized in electrochemical SERS systems for investigating electrode reactions on Pd surfaces.

DOI: 10.1021/acsami.5b02113
ACS Appl. Mater. Interfaces 2015, 7, 7129−7135

4. CONCLUSIONS

We have demonstrated that nanoflake Pd structures can be prepared via a simple electrodeposition on clean Au surfaces without additives or premodification of the substrate surfaces. Control of the deposition charge enabled regulation of the fine structure of the nanoflake Pd, and the effects of these structural changes on the water wettability and SERS activity were investigated. The wettability of the nanostructured Pd surfaces in terms of the water CA is closely correlated to the fine structures of Pd deposits and their surface roughness. Well-defined nanoflake Pd structures exhibited a superhydrophobic nature, with a CA of 160°. The effect of structural changes of the nanoflake Pd on the SERS activity was also examined, where the presence of sharp edge sites on Pd structures played a critical role in inducing high SERS activity. Well-defined nanoflake Pd structures exhibited good SERS reproducibility and stability in an electrochemical environment. The results demonstrated in this work regarding the effect of metal structures on the surface characteristics, wettability and SERS activity provide insights into the fabrication of functional metal nanostructures.

■ ASSOCIATED CONTENT

Ⓢ Supporting Information

Additional SEM images, cyclic voltammograms, contact-angle profile, and SERS spectra as noted in the text. This material is available free of charge via the Internet at http://pubs.acs.org.

■ AUTHOR INFORMATION

Corresponding Author

*J. Kim. E-mail: jongwonkim@chungbuk.ac.kr.

Notes

The authors declare no competing financial interest.

■ ACKNOWLEDGMENTS

This work was supported by the National Research Foundation of Korea (NRF) grant funded by the Korea government (MSIP) (No. 2014R1A2A1A11050622).

■ REFERENCES

(1) Katz, E.; Willner, I.; Wang, J. Electroanalytical and Bioelectroanalytical Systems Based on Metal and Semiconductor Nanoparticles. *Electroanalysis* **2004**, *16*, 19−44.

(2) Shipway, A. N.; Katz, E.; Willner, I. Nanoparticle Arrays on Surfaces for Electronic, Optical, and Sensor Applications. *ChemPhysChem* **2000**, *1*, 18−52.

(3) Solla-Gullon, J.; Vidal-Iglesias, F. J.; Feliu, J. M. Shape Dependent Electrocatalysis. *Annu. Rep. Prog. Chem., Sect. C: Phys. Chem.* **2011**, *107*, 263−297.

(4) Chen, J. Y.; Lim, B.; Lee, E. P.; Xia, Y. N. Shape-Controlled Synthesis of Platinum Nanocrystals for Catalytic and Electrocatalytic Applications. *Nano Today* **2009**, *4*, 81−95.

(5) Feng, J.-J.; Li, A.-Q.; Lei, Z.; Wang, A.-J. Low-Potential Synthesis of "Clean" Au Nanodendrites and Their High Performance toward Ethanol Oxidation. *ACS Appl. Mater. Interfaces* **2012**, *4*, 2570−2576.

(6) Velev, O. D.; Gupta, S. Materials Fabricated by Micro- and Nanoparticle Assembly—The Challenging Path from Science to Engineering. *Adv. Mater.* **2009**, *21*, 1897−1905.

(7) Wang, L. B.; Xu, L. G.; Kuang, H.; Xu, C. L.; Kotov, N. A. Dynamic Nanoparticle Assemblies. *Acc. Chem. Res.* **2012**, *45*, 1916−1926.

(8) Kleijn, S. E. F.; Lai, S. C. S.; Koper, M. T. M.; Unwin, P. R. Electrochemistry of Nanoparticles. *Angew. Chem., Int. Ed.* **2014**, *53*, 3558−3586.

(9) Plowman, B. J.; Bhargava, S. K.; O'Mullane, A. P. Electrochemical Fabrication of Metallic Nanostructured Electrodes for Electroanalytical Applications. *Analyst* **2011**, *136*, 5107−5119.

(10) Caputo, G.; Cortese, B.; Nobile, C.; Salerno, M.; Cingolani, R.; Gigli, G.; Cozzoli, P. D.; Athanassiou, A. Reversibly Light-Switchable Wettability of Hybrid Organic/Inorganic Surfaces with Dual Micro-/Nanoscale Roughness. *Adv. Funct. Mater.* **2009**, *19*, 1149−1157.

(11) Yang, C.; Tartaglino, U.; Persson, B. N. J. Influence of Surface Roughness on Superhydrophobicity. *Phys. Rev. Lett.* **2006**, *97*, 116103.

(12) Zhang, Q.-X.; Chen, Y.-X.; Guo, Z.; Liu, H.-L.; Wang, D.-P.; Huang, X.-J. Bioinspired Multifunctional Hetero-Hierarchical Micro/Nanostructure Tetragonal Array with Self-Cleaning, Anticorrosion, and Concentrators for the SERS Detection. *ACS Appl. Mater. Interfaces* **2013**, *5*, 10633−10642.

(13) Wang, G.; Zhang, T.-Y. Easy Route to the Wettability Cycling of Copper Surface between Superhydrophobicity and Superhydrophilicity. *ACS Appl. Mater. Interfaces* **2011**, *4*, 273−279.

(14) Wang, L.; Guo, S. J.; Hu, X. G.; Dong, S. J. Facile Electrochemical Approach to Fabricate Hierarchical Flowerlike Gold Micro Structures: Electrodeposited Superhydrophobic Surface. *Electrochem. Commun.* **2008**, *10*, 95−99.

(15) Ye, W.; Liu, J.; Liu, Q.; Zhou, F.; Liu, W. Surfactant-Free and Controllable Synthesis of Hierarchical Platinum Nanostructures and Their Comparative Studies in Electrocatalysis, Surface-enhanced Raman Scattering and Surface Wettability. *Electrochim. Acta* **2010**, *55*, 8649−8654.

(16) Zhang, H.; Xu, J. J.; Chen, H. Y. Shape-Controlled Gold Nanoarchitectures: Synthesis, Superhydrophobicity, and Electrocatalytic Properties. *J. Phys. Chem. C* **2008**, *112*, 13886−13892.

(17) Mengnan, Q.; Guangyu, Z.; Qi, W.; Xiaoping, C.; Junyan, Z. Fabrication of Superhydrophobic Surfaces by a Pt Nanowire Array on Ti/Si Substrates. *Nanotechnology* **2008**, *19*, 199801.

(18) Zhong, C. J.; Zak, J.; Porter, M. D. Voltammetric Reductive Desorption Characteristics of Alkanethiolate Monolayers at Single Crystal Au(111) and (110) Electrode Surfaces. *J. Electroanal. Chem.* **1997**, *421*, 9−13.

(19) Kudelski, A. Analytical Applications of Raman Spectroscopy. *Talanta* **2008**, *76*, 1−8.

(20) Choi, S.; Ahn, M.; Kim, J. Highly Reproducible Surface-enhanced Raman Scattering-Active Au Nanostructures Prepared by Simple Electrodeposition: Origin of Surface-enhanced Raman Scattering Activity and Applications as Electrochemical Substrates. *Anal. Chim. Acta* **2013**, *779*, 1−7.

(21) Plowman, B.; Ippolito, S. J.; Bansal, V.; Sabri, Y. M.; O'Mullane, A. P.; Bhargava, S. K. Gold Nanospikes Formed through a Simple Electrochemical Route with High Electrocatalytic and Surface Enhanced Raman Scattering Activity. *Chem. Commun.* **2009**, 5039−5041.

(22) Sharma, D. K.; Ott, A.; O'Mullane, A. P.; Bhargava, S. K. The Facile Formation of Silver Dendritic Structures in the Absence of Surfactants and Their Electrochemical and SERS Properties. *Colloids and Surf., A* **2011**, *386*, 98−106.

(23) Tian, N.; Zhou, Z. Y.; Sun, S. G.; Cui, L.; Ren, B.; Tian, Z. Q. Electrochemical Preparation of Platinum Nanothorn Assemblies with High Surface Enhanced Raman Scattering Activity. *Chem. Commun.* **2006**, 4090−4092.

(24) Xu, D.; Yan, X.; Diao, P.; Yin, P. Electrodeposition of Vertically Aligned Palladium Nanoneedles and Their Application as Active Substrates for Surface-enhanced Raman Scattering. *J. Phys. Chem. C* **2014**, *118*, 9758−9768.

(25) Liu, Z.; Yang, Z.-L.; Cui, L.; Ren, B.; Tian, Z.-Q. Electrochemically Roughened Palladium Electrodes for Surface-enhanced Raman Spectroscopy: Methodology, Mechanism, and Application. *J. Phys. Chem. C* **2007**, *111*, 1770−1775.

(26) Lee, H. K.; Lee, Y. H.; Zhang, Q.; Phang, I. Y.; Tan, J. M. R.; Cui, Y.; Ling, X. Y. Superhydrophobic Surface-Enhanced Raman Scattering Platform Fabricated by Assembly of Ag Nanocubes for Trace Molecular Sensing. *ACS Appl. Mater. Interfaces* **2013**, *5*, 11409−11418.

DOI: 10.1021/acsami.5b02113
ACS Appl. Mater. Interfaces 2015, 7, 7129−7135

(27) Shen, Y.; Wang, J.; Kuhlmann, U.; Hildebrandt, P.; Ariga, K.; Möhwald, H.; Kurth, D. G.; Nakanishi, T. Supramolecular Templates for Nanoflake−Metal Surfaces. *Chem.—Eur. J.* **2009**, *15*, 2763−2767.
(28) Bard, A. J.; Parsons, R.; Jordan, J. *Standard Potentials in Aqueous Solution*; Marcel Dekker: New York, 1985.
(29) Guo, S.; Wang, L.; Wang, E. Templateless, Surfactantless, Simple Electrochemical Route to Rapid Synthesis of Diameter-Controlled 3D Flowerlike Gold Microstructure with "Clean" Surface. *Chem. Commun.* **2007**, 3163−3165.
(30) Jia, F.; Wong, K.-w.; Zhang, L. Electrochemical Synthesis of Nanostructured Palladium of Different Morphology Directly on Gold Substrate through a Cyclic Deposition/Dissolution Route. *J. Phys. Chem. C* **2009**, *113*, 7200−7206.
(31) Li, Y.; Lu, G.; Wu, X.; Shi, G. Electrochemical Fabrication of Two-Dimensional Palladium Nanostructures as Substrates for Surface Enhanced Raman Scattering. *J. Phys. Chem. B* **2006**, *110*, 24585−24592.
(32) Xiao, L.; Zhuang, L.; Liu, Y.; Lu, J. T.; Abruna, H. D. Activating Pd by Morphology Tailoring for Oxygen Reduction. *J. Am. Chem. Soc.* **2009**, *131*, 602−608.
(33) Lafuma, A.; Quere, D. Superhydrophobic States. *Nat. Mater.* **2003**, *2*, 457−460.
(34) Darmanin, T.; de Givenchy, E. T.; Amigoni, S.; Guittard, F. Superhydrophobic Surfaces by Electrochemical Processes. *Adv. Mater.* **2013**, *25*, 1378−1394.
(35) Zhang, X.; Shi, F.; Yu, X.; Liu, H.; Fu, Y.; Wang, Z. Q.; Jiang, L.; Li, X. Y. Polyelectrolyte Multilayer as Matrix for Electrochemical Deposition of Gold Clusters: Toward Super-Hydrophobic Surface. *J. Am. Chem. Soc.* **2004**, *126*, 3064−3065.
(36) Zhao, N.; Shi, F.; Wang, Z.; Zhang, X. Combining Layer-by-Layer Assembly with Electrodeposition of Silver Aggregates for Fabricating Superhydrophobic Surfaces. *Langmuir* **2005**, *21*, 4713−4716.
(37) Yuan, Y.; Lee, T. R. In *Surface Science Techniques*; Bracco, G., Holst, B., Eds.; Springer: Berlin/Heidelberg, 2013; Vol. *51*, pp 3−34.
(38) Bhushan, B. Bioinspired Structured Surfaces. *Langmuir* **2012**, *28*, 1698−1714.
(39) Brolo, A. G.; Irish, D. E.; Szymanski, G.; Lipkowski, J. Relationship between SERS Intensity and Both Surface Coverage and Morphology for Pyrazine Adsorbed on a Polycrystalline Gold Electrode. *Langmuir* **1998**, *14*, 517−527.
(40) Hao, F.; Nehl, C. L.; Hafner, J. H.; Nordlander, P. Plasmon Resonances of a Gold Nanostar. *Nano Lett.* **2007**, *7*, 729−732.
(41) You, H.; Ji, Y.; Wang, L.; Yang, S.; Yang, Z.; Fang, J.; Song, X.; Ding, B. Interface Synthesis of Gold Mesocrystals with Highly Roughened Surfaces for Surface-enhanced Raman Spectroscopy. *J. Mater. Chem.* **2012**, *22*, 1998−2006.
(42) Choi, S.; Jeong, H.; Choi, K.-h.; Song, J. Y.; Kim, J. Electrodeposition of Triangular Pd Rod Nanostructures and Their Electrocatalytic and SERS Activities. *ACS Appl. Mater. Interfaces* **2014**, *6*, 3002−3007.
(43) Chen, L.-M.; Liu, Y.-N. Palladium Crystals of Various Morphologies for SERS Enhancement. *CrystEngComm* **2011**, *13*, 6481−6487.
(44) Cai, W. B.; Ren, B.; Li, X. Q.; She, C. X.; Liu, F. M.; Cai, X. W.; Tian, Z. Q. Investigation of Surface-enhanced Raman Scattering from Platinum Electrodes Using a Confocal Raman Microscope: Dependence of Surface Roughening Pretreatment. *Surf. Sci.* **1998**, *406*, 9−22.
(45) Abdelsalam, M. E.; Mahajan, S.; Bartlett, P. N.; Baumberg, J. J.; Russell, A. E. SERS at Structured Palladium and Platinum Surfaces. *J. Am. Chem. Soc.* **2007**, *129*, 7399−7406.
(46) McLellan, J. M.; Xiong, Y.; Hu, M.; Xia, Y. Surface-enhanced Raman Scattering of 4-Mercaptopyridine on Thin Films of Nanoscale Pd Cubes, Boxes, and Cages. *Chem. Phys. Lett.* **2006**, *417*, 230−234.
(47) Gómez, R.; Pérez, J. M.; Solla-Gullón, J.; Montiel, V.; Aldaz, A. In Situ Surface Enhanced Raman Spectroscopy on Electrodes with Platinum and Palladium Nanoparticle Ensembles. *J. Phys. Chem. B* **2004**, *108*, 9943−9949.
(48) Natan, M. J. Concluding Remarks - Surface Enhanced Raman Scattering. *Faraday Discuss.* **2006**, *132*, 321−328.

DOI: 10.1021/acsami.5b02113
ACS Appl. Mater. Interfaces 2015, 7, 7129−7135